Volume 19, Number 3, 2026. pp. 313-323

Jordan Journal of Physics

ARTICLE

Effects of Epoxy Resin 478 Coating Layer on the Field Electron Emission Performance of Carbon Fiber Emitters

Ali F. AlQaisi[a], **Adel M. Abuamr**[b], **M-Ali AL-Akhras**[c], **Saleh R. Al-Bashaish**[d], **Enas A. Arrasheed**[a] and **Marwan S. Mousa**[a]

[a] *Dept. of Renewable Energy Engineering, Jadara University, Irbid 21110, Jordan.*

[b] *Department of Mechanical Engineering and Manitoba Institute for Materials, University of Manitoba, Winnipeg, MB R3T 5V6, Canada.*

[c] *Department of Physical Sciences, Jordan University of Science & Technology, Irbid, 22110, Jordan.*

[d] *Department of Allied Sciences, Faculty of Arts and Sciences, Al-Ahliyya Amman University, Amman19328, Jordan.*

DOI: **https://doi.org/10.47011/19.3.3**

Received on: 11/03/2025; *Accepted on: 08/01/2026*

Abstract: This study investigates the field electron emission from the polyacrylonitrile (PAN) carbon fiber (VPR-19, treated at 2800°C) before and after applying a coating layer of an insulating material (single-component epoxy resin). The study includes the measurement of the current-voltage characteristics and analyzing the results using the Murphy-Good plots. High-resolution spectroscopic electron micrographs and emission distribution patterns were also recorded. Moreover, the ultraviolet photoelectron spectroscopy technique was used to measure the work function of the carbon fibers as it is an essential requirement to obtain the analysis results. The study found that coated emitters showed significant improvements in emission current characteristics compared with uncoated emitters.

Keywords: Field electron emission, Carbon fiber, E478 epoxy resin, Coated carbon fiber, Field emission tips.

1. Introduction

Field electron emission (FEE) transpires when a substantial electric field is applied to an emitter's surface to extract free electrons [1–3]. The released electrons traverse the potential barrier [4–7]. This phenomenon arises from quantum mechanical tunneling [8–12].

Industry and academia alike are interested in carbon-based structures as cold cathodes for cutting-edge applications. Many efforts have examined and sought to comprehend the field-emission characteristics of these materials. The reliability of theoretical field-emission models has also been tested in various ways. Some of the well-known cathodes reported in the literature were fabricated from several types of carbon-based materials such as graphite [13], graphene [14], multiwalled and single-walled carbon nanotubes [15–18], carbon nanoparticles [19, 35], and carbon fibers (CF) [20–27]. Carbon-based and hybrid nanomaterials have also been investigated in other advanced energy-conversion devices, including perovskite-based solar cells using multilayer and band-gap engineering approaches [38]. Their low turn-on electrostatic field, high emission current density, current stability, and rapid pulse repetition rate are just a few of their appealing field emission characteristics.

Among various carbon allotropes, CFs represent a promising class of cold-cathode

Corresponding Author: Marwan S. Mousa **Email**: m.mousa@jadara.edu.jo

emitters because they are inexpensive, mechanically stable, and easily integrated into miniaturized electronic devices. For example, cathodes made of CF cathodes can emit stable currents for long periods despite low vacuum conditions, and they are more resistant to ion bombardment than metal emitters [28].

Nevertheless, pristine CFs often suffer from surface irregularities, uncontrolled emission sites, localized heating, and long-term degradation, all of which reduce the emission stability and efficiency. To overcome these limitations, several surface-engineering approaches have been previously investigated, such as the deposition of metallic films and the application of oxide coatings or polymeric dielectric layers [29, 30]. Recent work on composite cold-field emission emitters has also demonstrated that epoxy-coated microtips can exhibit measurable dielectric and impedance responses, highlighting the importance of the electrical properties of the coating layer in composite emitter structures [36].

Polymeric coatings such as polystyrene and PMMA have been shown to reduce the operating voltage and improve emission uniformity by introducing a dielectric barrier. For example, Fawaeer et al. [22] achieved improved current stability using polystyrene-modified fibers, while Park et al. [16, 17] reported moderate enhancement with PMMA layers. Despite these improvements, such coatings typically suffer from limited dielectric strength, weak thermal resistance, and poor long-term stability under high electric fields.

Unlike earlier polymer coatings, this work introduces Elantas epoxylite E478 single-component epoxy resin (E478 for simplicity, produced by Elantas Europe) as a dielectric coating for CF emitters [31]. Single-component epoxy resins offer several advantages over polystyrene and PMMA, including higher dielectric strength, superior thermal and chemical stability, stronger interfacial adhesion to the carbon surface, and a cross-linked molecular structure that enables more uniform charge trapping and redistribution [37].

The ultraviolet photoelectron spectroscopy (UPS) technique was used to measure the work function (ϕ) of the carbon fibers. ϕ is an essential parameter in field emission science as it describes the potential energy barrier where the quantum tunneling mechanism of the emission process takes place. The electronic structure of the E478 epoxy resin was studied before by Allaham [31], and we are referring to his $\phi_{478} = 3.42$ eV result for the epoxy resin.

These attributes are expected to significantly enhance field emission performance and operational stability. The results presented in this study establish a direct quantitative comparison between epoxy-coated CF emitters and both uncoated CFs and previously reported polymer-coated emitters. This provides a new insight into the role of cross-linked dielectric coatings in stabilizing and enhancing electron emission.

2. Methodology

2.1. Sample Fabrication

2.1.1. CF Tips

Carbon polyacrylonitrile (PAN) fibers (VPR-19, treated at 2800 °C) with a diameter of 7 μm, a density of 1.85 g·cm^{-3}, and a carbon intensity of 68% were used to fabricate CF tips [32, 33]. The fibers were adhered to stainless steel tubes using silver conductive Adhesive 503 to ensure strong electrical conductivity. The samples were then etched with a 0.1 M solution of NaOH to fabricate nano-sized CF tips, while the etching process was controlled by selecting an initial etching current of 35 μA at 2 volts. The etching procedure was followed by an ultrasonic cleaning bath that is essential to remove any NaOH solution residues from the surface of the etched tip.

The CF tips were then examined with scanning electron microscope (SEM, Quanta FEG 450, Thermo Fisher Scientific, USA) to determine the validity of sample production and the radius of the tip apex. Fig. 1 shows the SEM images of the produced sample, showing a radius of curvature of ~35.35 nm.

2.1.2. CF-E478 Tips

After measuring the field-emission characteristics of the uncoated samples, the samples were coated with the E478 epoxy resin. To prepare the coating solution, the epoxy was mixed with ethanol to make a homogeneous solution in the ratio of (epoxy) 2:1 (ethanol). The coating technique involves slowly dipping the CF tip into the resin-ethanol mixture, then carefully withdrawing it to ensure that only a

thin layer of resin remains on the tip surface. The coating layer thickness is determined by calculating the difference between the radii of the coated and uncoated samples estimated by SEM. Fig. 2 shows the SEM image of the coated sample, with a radius of curvature of ~ 210.45 nm. Thus, the coating layer thickness was about ~175.1 nm. Table 1 shows the geometrical analysis results for three CF samples and the corresponding coating layer thickness.

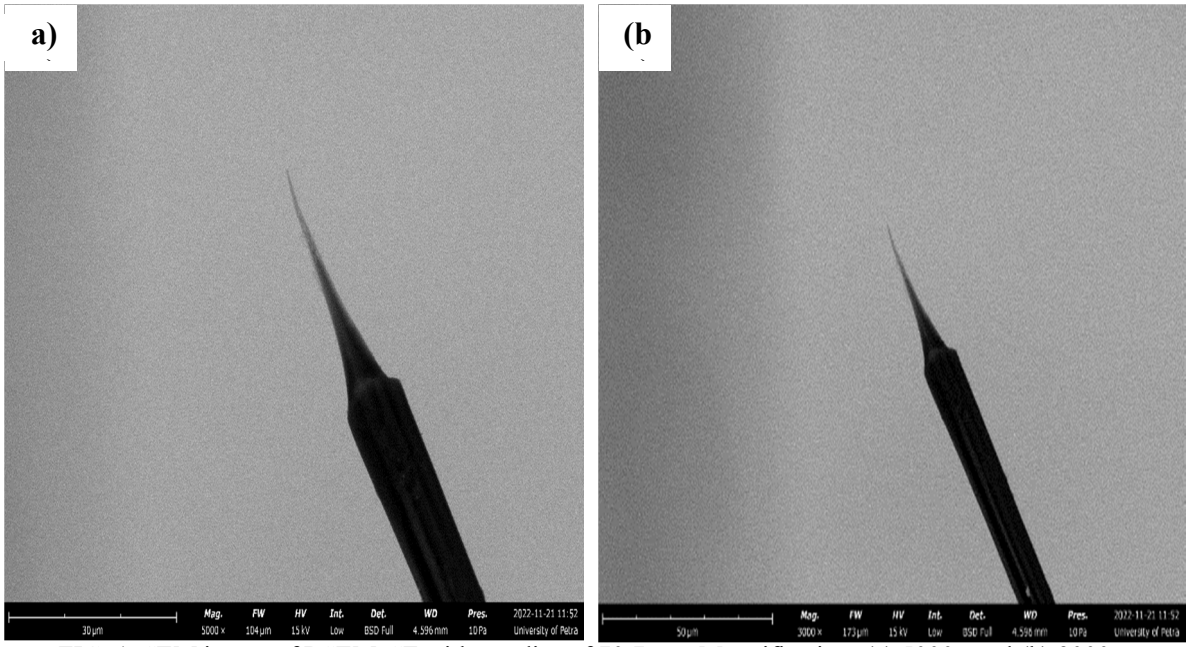

FIG. 1. SEM image of RSEM-CF with a radius of 70.7 nm. Magnification: (a) 5000x and (b) 3000x.

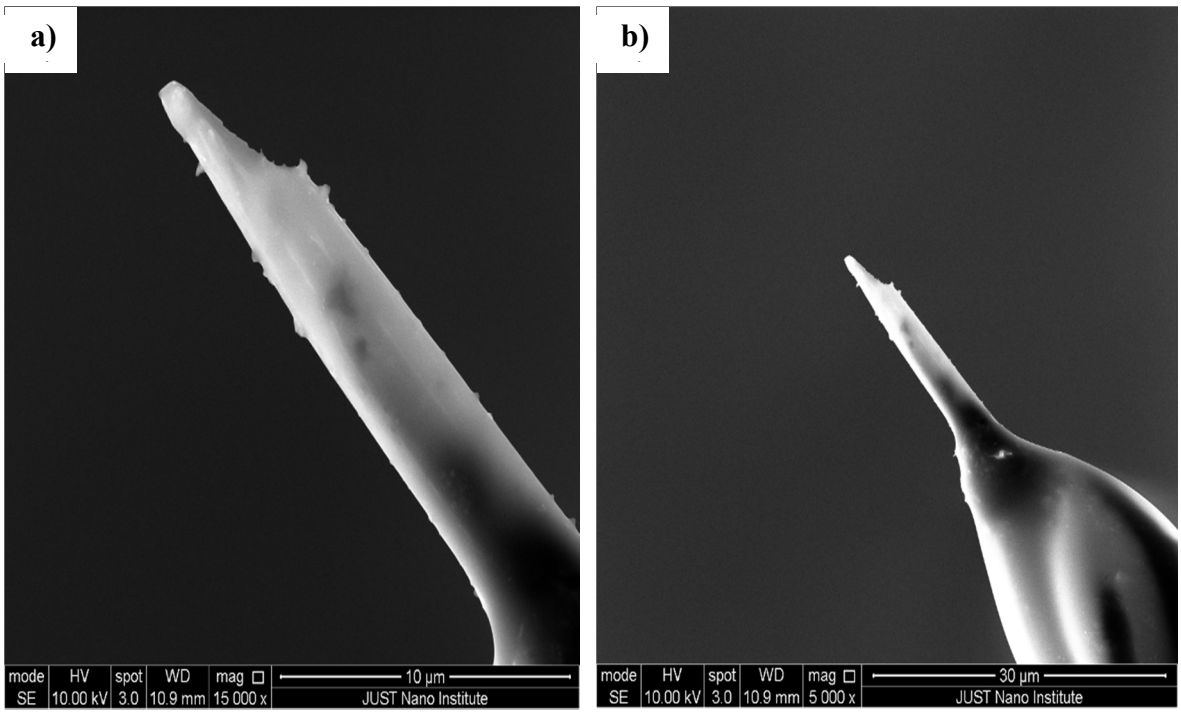

FIG. 2. SEM image of the CF- E478 composite. Magnification: (a) 15000x and (b) 5000x.

TABLE 1. Measured radii and coating layer thicknesses for the three carbon fiber samples.

Sample	Condition	Radius (nm)	Layer thickness (nm)
CF_1	Before coating	39.95	67.55
	After coating	107.5	
CF_2	Before coating	35.35	175.1
	After coating	210.45	
CF_3	Before coating	49.95	37.55
	After coating	87.5	

2.2 Experimental Setup

The samples were mounted in a home-built field emission microscope (FEM) with an ultrahigh-vacuum chamber supported by a pumping system consisting of a rotary and silicon oil diffusion pumps. The system also includes a thermal treatment setup and a liquid nitrogen trap, in addition to an ultrahigh-voltage feedthrough and a phosphorus screen.

The samples in this study were attached as the cathode to the system's high-voltage power supply (0–6.5 kV, FUG HCN 140-6500, Germany), while the phosphorus screen was grounded and attached as the anode of the system to collect the emitted electrons. The cathode-anode separation was 10 mm.

The emitted current was measured using the KEITHLEY 485 auto-ranging picoammeter, and the FEM pattern was captured using a Nikon D7500 digital camera. The experiments were conducted after a thermal treatment for 12 hours at ~180 °C inside a high-vacuum environment with a pressure of 10^{-6} mbar, achieved after immediate cooling with liquid nitrogen prior to the heating step. This procedure was followed for both types of fabricated samples (coated and uncoated).

3. Results and Discussions

The results of this study were obtained from three CF samples that were then coated to establish a comprehensive overview of the effect of coating the carbon fibers with the E478 epoxy resin. The three samples are labeled CF_1, CF_2, and CF_3, respectively.

The results contain the field emission characteristics presented by the current-voltage characteristics of a full voltage increase-decrease cycle that traces the behavior of the emitted current, in addition to the field emission current distribution that is described by the emission pattern. Moreover, the MG analyses are presented for each part of the current-voltage ($I(V)$) cycle.

3.1. Work Function of the Carbon Fibers

UPS was used to determine the work function ϕ for the samples. The work function can be calculated from the following relation:

$$\phi = 21.22 - W \quad (1)$$

In Eq. (1), 21.22 eV is the energy of the ultraviolet photons, W is the spectrum width between the first inflection point and the baseline starting point of the UPS spectrum [31]. The measured spectrum is presented in Fig. 3, and it measures $\phi_{\mathrm{CF}} = 4.19$ eV.

In the Murphy-Good (MG) analysis, the analysis plots have the form of $\ln\left(I.V^{-k(\phi)}\right)$ vs $1/V$, where $k(\phi)_{\mathrm{CF}} = 1.199114$ as determined from the Murphy-Good analysis [13]. The corresponding values for E478, as measured by Allaham, are $\phi_{478} = 3.42$ eV and $k(\phi)_{\mathrm{E478}} = 1.113529$. Note that the values were measured using the Field Emission Analysis Webtool explained in references [13] and [34].

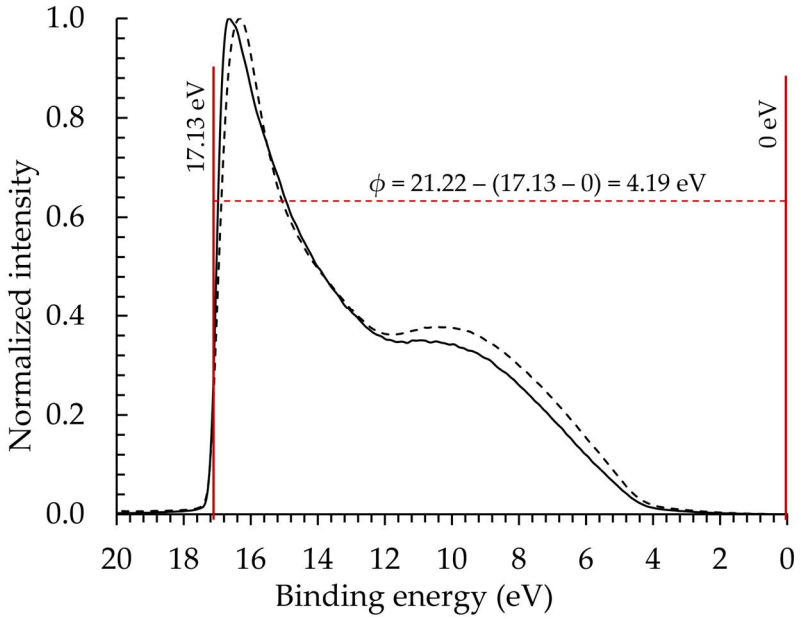

FIG. 3. UPS spectrum for the Carbon polyacrylonitrile (PAN) fibers (VPR-19, treated at 2800°C).

3.2 Emission Characteristics of the CF_1 Tip.

The $I(V)$ characteristics and the corresponding Murphy-Good analysis for the uncoated CF_1 sample are presented in Fig. 4. The full cycle of increasing (V_{inc}) and decreasing (V_{dec}) applied voltage is described in Fig. 4(a), while the corresponding MG-plots are presented in Fig. 4(b) for the full cycle.

The results show a threshold voltage of 500 V for V_{inc}, while it was shifted to 400 V in the case of V_{dec}. The maximum recorded emission current was 1.7 µA at 800 V. The MG-plots show one line segment for the case of V_{inc} case (L_1), which was split into three segments in the case of V_{dec} (L_2, L_3, and L_4). The slope of L_1 segment is –1324.1 Np.V, while the extracted field emission parameters were expressed in terms of the voltage conversion length ζ_C (26.4 nm) and the extracted formal emission area A_f (4×10^{-22} m^2) for single-tip emitters.

The slopes of the segments L_2, L_3, and L_4 are –520.9 Np.V, –756.6 Np.V, and 139.1 Np.V, respectively. Moreover, the extracted ζ_C and A_f values for this part of the cycle are valid only for L_2 and L_3 segments (L_4 is related to unorthodox emission conditions [13]), with values of 13.7 nm and 1×10^{-22} m^2 for L_2, along with 10 nm and 4×10^{-23} m^2 for L_3.

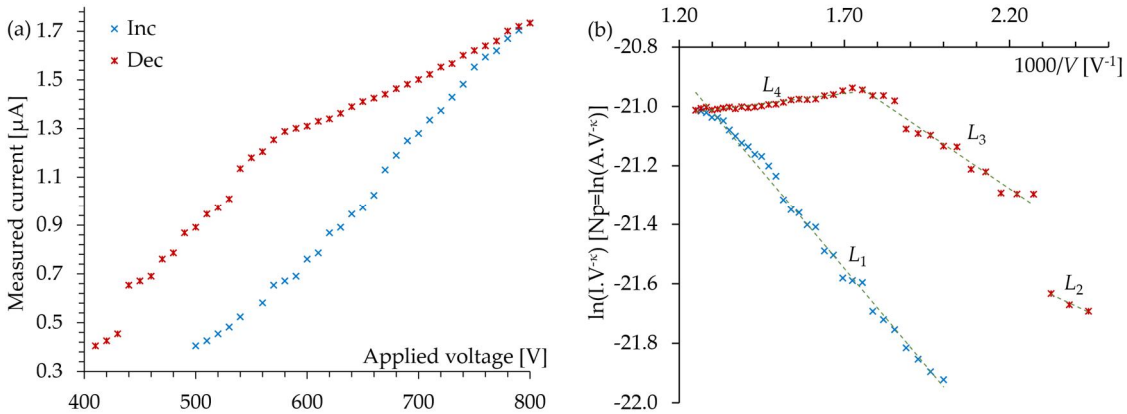

FIG. 4. (a) current-voltage characteristics and (b) corresponding Murphy-Good plots for the uncoated CF_1 sample.

During this cycle, several images of the emission pattern were recorded at different voltages, and the results are presented in Fig. 5. The results show an enhanced buildup of the emission pattern into a more focused shape as the voltage is increased.

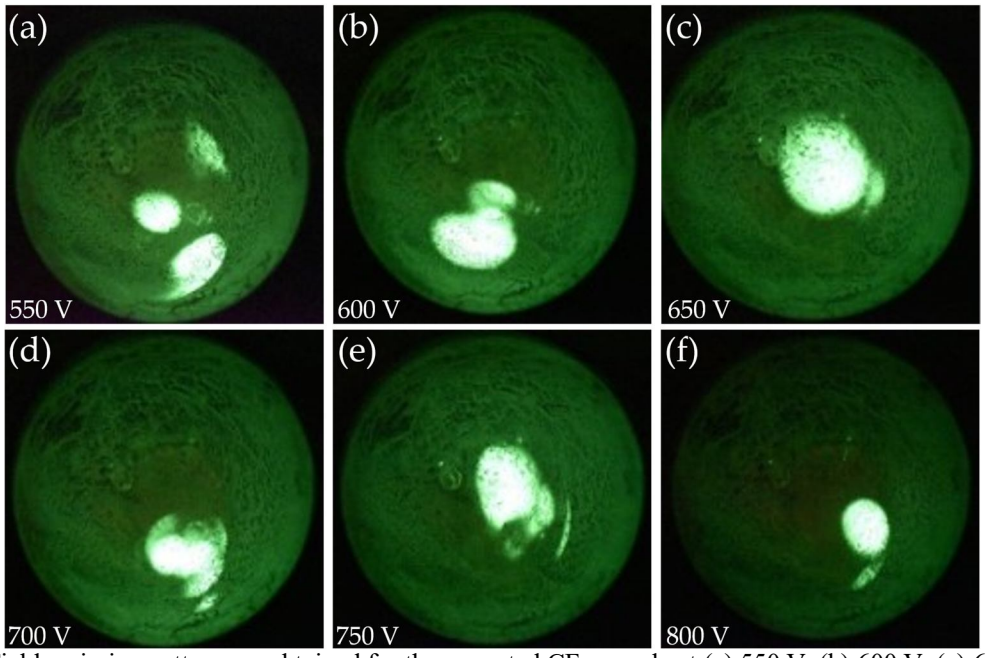

FIG. 5. Field emission patterns as obtained for the uncoated CF_1 sample at (a) 550 V, (b) 600 V, (c) 650 V, (d) 700 V, (e) 750 V, and (f) 800 V.

Fig. 6 presents the $I(V)$ characteristics of the coated CF1-E478 sample and the corresponding MG plots. In this case, the threshold voltage shifted down by 170 V compared to the uncoated CF1 sample, where the value was recorded at 330V for both parts of the cycle. However, the maximum emission current measured increased by 1.3 µA to reach 3 µA at 800 V. The MG-plot for the V_{inc} part of this cycle is described by three lines (L_1, L_2, and L_3). The slope of L_1 is –15989 Np.V, while the extracted ζ_C value is 309.6 nm, and the extracted A_f value is 13.1×10^{-4} m^2. The results for L_2 segment have a slope value of –1002.8 Np.V, ζ_C value of 21.1 nm, and A_f value of 4.3×10^{-22} m^2. Moreover, the slope for L_3 is –812.3 Np.V, along with ζ_C value of 19 nm, and A_f value of 3.1×10^{-22} m^2.

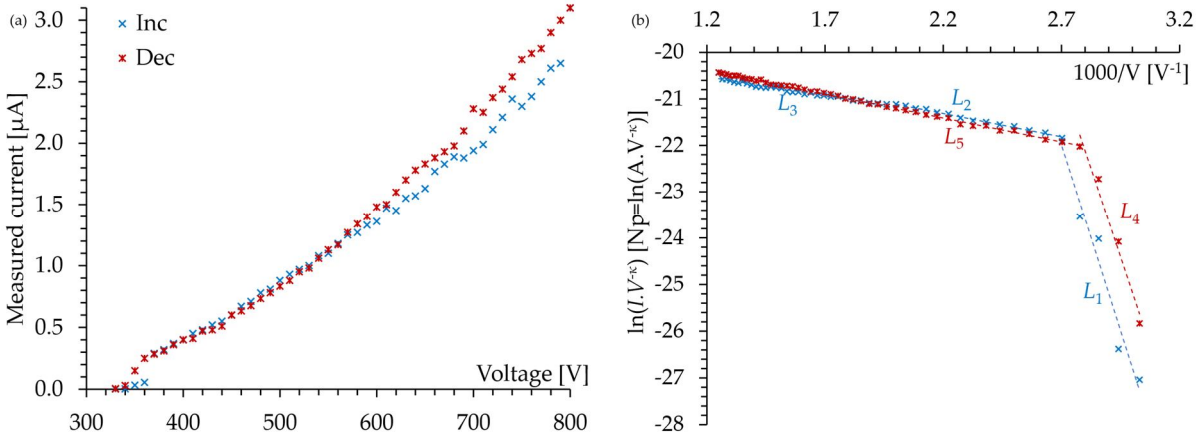

FIG. 6. (a) current-voltage characteristics and (b) corresponding Murphy-Good plots for the coated CF_1-E478 sample.

It is important to note that for segment L_1, both emission area and voltage conversion length values were much higher than for segments L_2 and L_3. Even though it was operating at lower voltages, the sample in the L_1 operating interval was more consistent with an orthodox field emission system. However, for L_2 and L_3 it is supposed to be more related to thermally assisted field emission behavior because of the classical tunneling of electrons through the epoxy layer.

The V_{dec} part of the cycle shows two linear segments, L_4 and L_5. The slopes of these segments are –15255 Np.V and –1030.2 Np.V, respectively. The extracted ζ_{C} and A_{f} values for the L_4 segment are 298.3 nm and 7.4×10^{-4} m^2, respectively, and 20.6 nm and 3.74×10^{-22} m^2 (respectively) for the L_5 segment. It is noted that, in the case of the coated samples, the emitters showed a more reversible emission behavior than the uncoated ones. This supports previously reported results showing enhanced emission from coated samples [22, 27, 32].

The field emission patterns that describe this cycle of applied voltages are presented in Fig. 7. The images show more bright spots at lower voltages, as the emission area was much higher than at higher voltages.

The current-voltage characteristics and the corresponding Murphy-Good plots for samples CF_2 and CF_3 are presented in Fig. 8 and Fig. 9, respectively. Moreover, the results are summarized in Table 2 for the threshold voltage and maximum operational current-voltage values, and in Table 3 for the MG analysis, comparing the results for the three tested samples.

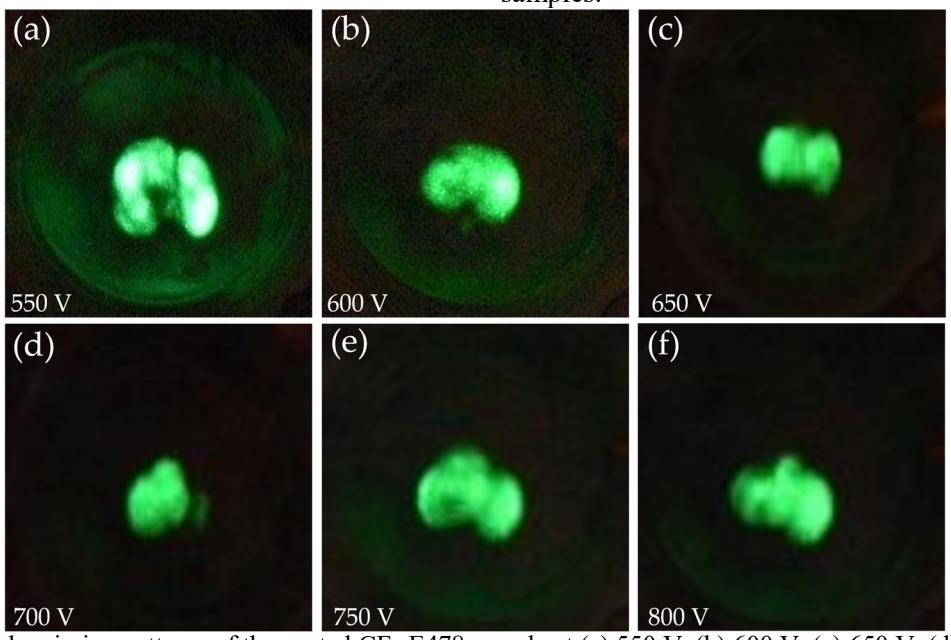

FIG. 7. Field emission patterns of the coated CF_1-E478 sample at (a) 550 V, (b) 600 V, (c) 650 V, (d) 700 V, (e) 750 V, and (f) 800 V.

TABLE 2. Summary of the current-voltage characteristics of the three samples.

Sample	Cycle part	$V_{\mathrm{threshold}}$ (V)	Maximum (V, I) (V, μA)
CF_1	V_{inc} V_{dec}	500 400	(800, 1.7)
CF_1-E478	V_{inc} V_{dec}	330 330	(800, 3)
CF_2	V_{inc} V_{dec}	210 140	(600, 2.4)
CF_2-E478	V_{inc} V_{dec}	Switch On at 750 V 250	(850, 3.28)
CF_3	V_{inc} V_{dec}	460 400	(800, 2.4)
CF_3-E478	V_{inc} V_{dec}	300 260	(800, 2.3)

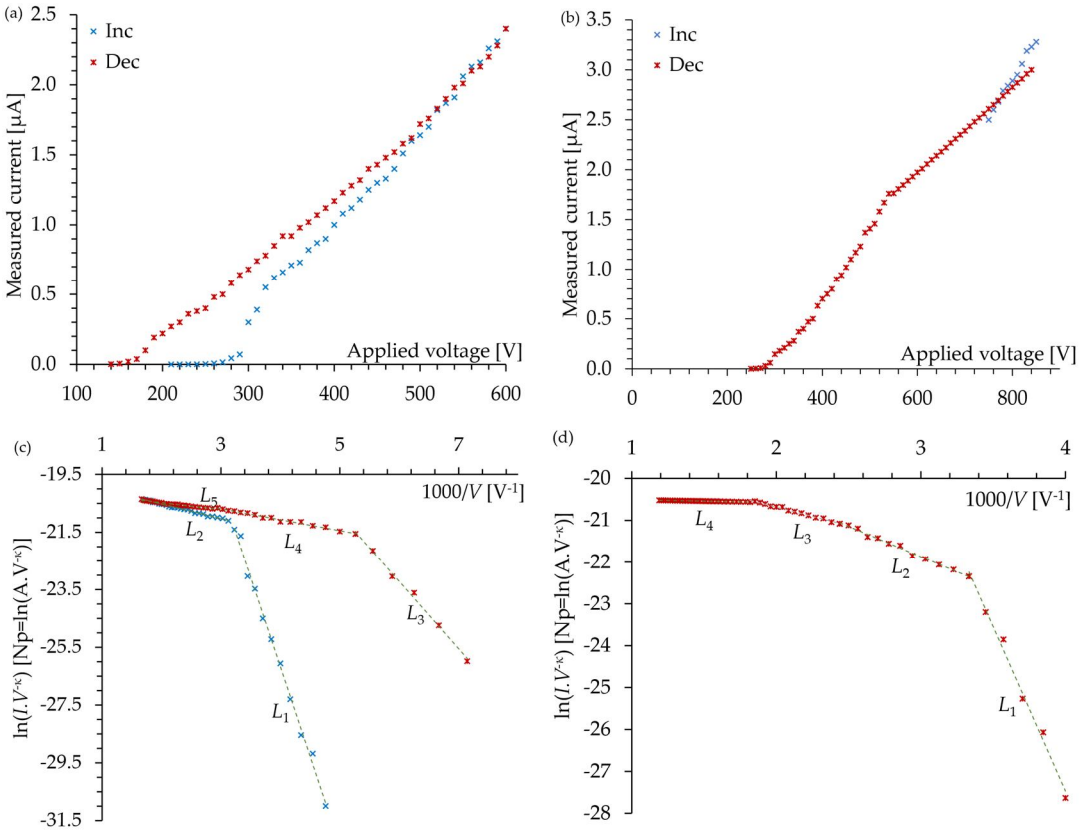

FIG. 8. Field emission characteristics for the CF_2 sample before and after coating: (a) current-voltage characteristics before coating, (b) current-voltage characteristics after coating, (c) Murphy-Good plot of (a), and Murphy-Good plot of (b).

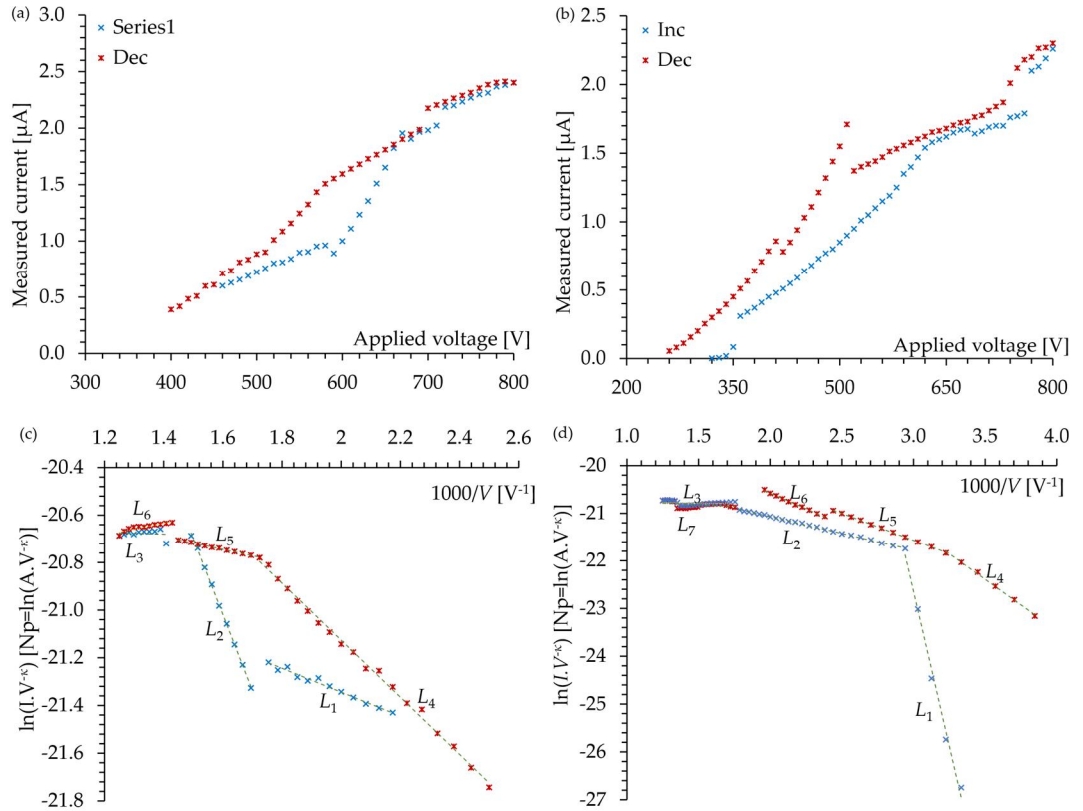

FIG. 9. Field emission characteristics for the CF_3 sample before and after coating: (a) current-voltage characteristics before coating, (b) current-voltage characteristics after coating, (c) Murphy-Good plot of (a), and Murphy-Good plot of (b).

TABLE 3. Murphy-Good analysis for a full voltage cycle for each sample.

Sample	Segment number	Slope [Np.V]	ζ_C [nm]	A_f [m^2]
CF_1	L_1	–1324.1	26.4	4.0×10^{-22}
	L_2	–520.9	13.7	1.0×10^{-22}
	L_3	–756.6	10.0	4.0×10^{-23}
	L_4	139.1	---	---
CF_1-E478	L_1	–15989.0	309.6	13.1×10^{-4}
	L_2	–1002.8	21.1	4.3×10^{-22}
	L_3	–812.3	19.0	3.1×10^{-22}
	L_4	–15255.0	298.3	7.4×10^{-4}
	L_5	–1030.2	20.6	3.7×10^{-22}
CF_2	L_1	–6206.7	136.4	3.0×10^{-10}
	L_2	–506.7	10.6	4.9×10^{-21}
	L_3	–2337.8	46.6	2.1×10^{-17}
	L_4	–379.1	76.4	8.0×10^{-23}
	L_5	–244.2	46.6	2.9×10^{-23}
CF_2-E478	L_1	–7848.7	156.8	4.8×10^{-11}
	L_2	–1452.1	28.0	2.4×10^{-21}
	L_3	–881.1	16.4	3.1×10^{-22}
	L_4	–63.1	3.6	1.6×10^{-22}
CF_3	L_1	–500.8	4.0	1.6×10^{-23}
	L_2	–3194.6	41.8	3.4×10^{-21}
	L_3	–36.9	4.2	9.6×10^{-24}
	L_4	–1197.0	24.7	7.8×10^{-22}
	L_5	–268.3	6.8	3.5×10^{-23}
	L_6	248.6	---	---
CF_3-E478	L_1	–12958.8	252.2	9.9×10^{-6}
	L_2	–706.9	14.0	1.4×10^{-22}
	L_3	–138.7	7.2	3.6×10^{-23}
	L_4	–2145.7	42.2	5.6×10^{-20}
	L_5	–1133.3	22.4	1.1×10^{-21}
	L_6	–1311.4	26.3	1.7×10^{-21}
	L_7	–58.0	1.0	1.9×10^{-21}

The results in Table 2 show that the three uncoated samples are almost identical, with slight shifts in threshold voltage that can be related to differences in tip-apex geometry. This proves that the followed preparation methodology produces samples with successful repeatability. As for coating, the first sample was dipped in the coating solution 6 times, the second 12 times, and the third 3 times. As a result, the second sample showed the expected switch-on phenomenon because of the thick layer (thickness of ~175.1 nm). However, for the first and third samples, it showed that the thickness of the coating layer was not sufficient to show such a behavior, but only a shift toward lower threshold voltages. This was reflected in the results as shown in Table 2 and Table 3, and in the behavior of the curves in Figures 4, 5, 8, and 9.

4. Conclusions

Carbon fiber field emission emitters were fabricated using an electrochemical etching technique. Their geometries were characterized using SEM, and the work function of the fibers was measured by ultraviolet photoelectron spectroscopy. After initial field emission measurements, the same samples were coated with varying numbers of layers of the Elantas single-component epoxy resin E478. The coated samples were then re-characterized using the same techniques. Field emission measurements were then repeated to assess how the epoxy coating influenced the emission behavior.

Murphy-Good analysis was employed to analyze the emission data, requiring accurate work function values, which were 4.19 eV for the uncoated fibers and 3.42 eV for the coated

ones. These values were used to generate the Murphy-Good plots for full current-voltage cycles. The characteristics and analysis results, summarized in Tables 1 and 2, indicate that carbon fiber emitters should ideally be operated at low voltages, with the applied voltage not exceeding ~300 V above the threshold value. Moreover, the coating process showed a switch-on phenomenon for the thick coating layer (> 200 nm), while it lowered the threshold voltages for thinner coatings.

References

[1] Stratton, R., Phys. Rev., 125 (1962) 67.

[2] Latham, R.V. and Mousa, M.S., J. Phys. D: Appl. Phys., 19 (1986) 699.

[3] Abuamr, A.M. et al., Physica Scripta, 99 (10) (2024) 105029.

[4] Murphy, E.L. and Good Jr, R.H., Physical Review, 102 (1956) 1464.

[5] Yanashima, R., Hirai, N., and Ohki, Y., "Effects of Addition of MgO Fillers with Various Sizes and Co-addition of Nano-sized SiO_2 Fillers on the Dielectric Properties of Epoxy Resin", vol. 2, (2017), pp 650–653.

[6] Lawrowski, R., Hausladen, M., Buchner, P., and Schreiner, R., IEEE Trans. Electron Devices, 68 (2021) 4116.

[7] Mousa, M.S., Arrasheed, E.A., Abuamr, A.M., Soud, A.A., and Sobola, D., 37th International Vacuum Nanoelectronics Conference (IVNC), (2024) 197309.

[8] Ławrowski, R., Bachmann, M., and Schreiner, R., Journal of Vacuum Science & Technology, 40 (2022).

[9] Mousa, M.S., Abuamr, A.M., Soud, A.A., Knápek, A., and Sobola, D., 37th International Vacuum Nanoelectronics Conference (IVNC), (2024) 201104.

[10] Peillon, S. et al., J. Aerosol Sci., 137 (2019) 105431.

[11] Al Soud, A. et al., 37th International Vacuum Nanoelectronics Conference (IVNC), (2024) 272373584.

[12] Stern, T.E., Gossling, B.S., and Fowler, R.H., Proc. A, 124 (795) (1929) 699.

[13] Allaham, M.M. et al., Surfaces and Interfaces, 53 (2024) 105102.

[14] Chen, L., Yu, H., Zhong, J., Song, L., Wu, J., and Su, W., Materials Science and Engineering: B, 220 (2017) 44.

[15] Popov, E.O., Kolosko, A.G., Filippov, S.V., and de Assis, T.A., Vacuum, 173 (2020) 109159.

[16] Posos, T.Y., Fairchild, S.B., Park, J., and Baryshev, S.V., J. Vac. Sci. Technol. B, 38 (2) (2020) 024006.

[17] Fairchild, S.B., Zhang, P., Park, J., Back, C.T., Marincel, D., Huang, Z., and Pasquali, M., IEEE Trans. Plasma Sci., 47 (5) (2019) 2032.

[18] Mousa, M.S. and Daradkeh, S.I., Jordan J. Phys., 12 (1) (2019) 87.

[19] Al-Braikat, H.A. et al., Karbala International Journal of Modern Science, 10 (2) (2024) Article 3.

[20] Mousa, M.S., Surf. Sci., 94/95 (1996) 129.

[21] Mousa, M.S., Ultramicroscopy, 73 (1) (1998) 23–30.

[22] Fawaeer, S., Shatnaw, M., Allaham, M., and Mousa, M., Advances in Materials and Processing Technologies, 8 (3) (2022) 2775.

[23] Baker, V.S., Osborne, A.R., and Williams, J., J. Phys. D: Appl. Phys., 7 (1974) 2105.

[24] Braun, E., Smith, J.F., and Sykes, D.E., Vacuum, 25 (1975) 425.

[25] Moran, J.A. et al., Carbon, 86 (2015) 363.

[26] Bondarenko, B.V., Rybakov, Y.L., and Sheshin, E.P., Radiotechnika (Moscow), 27 (1982) 1593.

[27] Mousa, M.S. and Kelly, T.F., Ultramicroscopy, 95 (2003) 125.

[28] Chouhan, V., Noguchi, T., and Kato, S., J. Appl. Phys., 119 (13) (2016) 134303.

[29] Giubileo, F., Di Bartolomeo, A., Iemmo, L., Luongo, G., and Urban, F., Applied Sciences, 8 (4) (2018) 526.

[30] Dwivedi, N. et al., Journal of Materials Chemistry C, 9 (8) (2021) 2620.

[31] Allaham, M.M., ACS Omega, 9 (28) (2024) 30975.

[32] Almasri, A.M., Hagmann, M.J., and Mousa, M.S., "Applied Microscopy", (2017).

[33] Virgil'ev, Y.S. and Kalyagina, I.P., Inorganic Materials, 40 (Suppl. 1) (2004) S33.

[34] Allaham, M., Knápek, A., Mousa, M., and Forbes, R., 34th International Vacuum Nanoelectronics Conference (IVNC), Virtual conf. hosted in Lyon, France, (2021).

[35] Al-Bashaish, S.R. et al., Materials Science and Engineering: B, 323 (2026) 118772.

[36] Alsoud, A., Shaheen, A.A., Knápek, A., Al-Bashaish, S.R., Ahmad, M.D.J., Mousa, M.S., and Sobola, D., ACS Omega, 10 (11) (2025) 11108–11118.

[37] Alsoud, A. et al., Physica Scripta, 99 (2024) 116101.

[38] Al Dmour, H. et al., Proceedings of the Romanian Academy Series A, 26 (1) (2025) 53–61.